Journal of Biomechanics 128 (2021) 110726

Contents lists available at ScienceDirect

Journal of Biomechanics

journal homepage: www.elsevier.com/locate/jbiomech

Association between bone shape and the presence of a fracture in patients with a clinically suspected scaphoid fracture

Melissa S.A.M. Bevers [a,b,c], Caroline E. Wyers [a,b,d], Anne M. Daniels [b,e], Emmanuel A. Audenaert [f,g], Sander M.J. van Kuijk [h], Bert van Rietbergen [c,i], Piet P.M. M. Geusens [d,j], Sjoerd Kaarsemaker [k], Heinrich M.J. Janzing [e], Pascal F.W. Hannemann [l], Martijn Poeze [b,l], Joop P. van den Bergh [a,b,d,j,*]

[a] Department of Internal Medicine, VieCuri Medical Center, Venlo, the Netherlands
[b] NUTRIM School for Nutrition and Translational Research in Metabolism, Faculty of Health Medicine and Life Sciences, Maastricht University Medical Center, Maastricht, the Netherlands
[c] Orthopedic Biomechanics, Department of Biomedical Engineering, Eindhoven University of Technology, Eindhoven, the Netherlands
[d] Department of Internal Medicine, Subdivision of Rheumatology, Maastricht University Medical Center, Maastricht, the Netherlands
[e] Department of Surgery, VieCuri Medical Center, Venlo, the Netherlands
[f] Department of Orthopedic Surgery and Traumatology, Ghent University Hospital, Ghent, Belgium
[g] Department of Electromechanics, Op3Mech research group, University of Antwerp, Antwerp, Belgium
[h] Department of Clinical Epidemiology and Medical Technology Assessment, Maastricht University Medical Center, Maastricht, the Netherlands
[i] Department of Orthopedic Surgery, Maastricht University Medical Center, Maastricht, the Netherlands
[j] Faculty of Medicine and Life Sciences, Hasselt University, Belgium
[k] Department of Orthopedic Surgery, VieCuri Medical Center, Venlo, the Netherlands
[l] Department of Surgery and Trauma Surgery, Maastricht University Medical Center, Maastricht, the Netherlands

ARTICLE INFO

Keywords:
Scaphoid fracture
Bone shape
Statistical shape modeling
High-resolution peripheral quantitative computed tomography

ABSTRACT

Scaphoid fractures are difficult to diagnose with current imaging modalities. It is unknown whether the shape of the scaphoid bone, assessed by statistical shape modeling, can be used to differentiate between fractured and non-fractured bones. Therefore, the aim of this study was to investigate whether the presence of a scaphoid fracture is associated with shape modes of a statistical shape model (SSM). Forty-one high-resolution peripheral quantitative computed tomography (HR-pQCT) scans were available from patients with a clinically suspected scaphoid fracture of whom 15 patients had a scaphoid fracture. The scans showed no motion artefacts affecting bone shape. The scaphoid bones were semi-automatically contoured, and the contours were converted to triangular meshes. The meshes were registered, followed by principal component analysis to determine mean shape and shape modes describing shape variance. The first five out of the forty shape modes cumulatively explained 87.8% of the shape variance. Logistic regression analysis was used to study the association between shape modes and fracture presence. The regression models were used to classify the 41 scaphoid bones as fractured or non-fractured using a cut-off value that maximized the sum of sensitivity and specificity. The classification of the models was compared with fracture diagnosis on HR-pQCT. A regression model with four shape modes had an area under the ROC-curve of 72.3% and correctly classified 75.6% of the scaphoid bones (fractured: 60.0%, non-fractured: 84.6%). To conclude, fracture presence in patients with a clinically suspected scaphoid fracture appears to be associated with the shape of the scaphoid bone.

1. Introduction

Scaphoid fractures are the most common carpal bone fractures, and they are difficult to diagnose. These fractures account for 60–75% of all carpal bone fractures and predominantly occur in a young and active male population (Duckworth et al., 2012b; Hove, 1999; Van Onselen et al., 2003; Van Tassel et al., 2010). Unnecessary treatment is frequent due to, amongst other reasons, a high false-positive rate with currently

* Corresponding author.at: VieCuri Medical Center - Department of Internal Medicine, Tegelseweg 210, Venlo 5912 BL, The Netherlands.
E-mail address: jvdbergh@viecuri.nl (J.P. van den Bergh).

https://doi.org/10.1016/j.jbiomech.2021.110726
Accepted 9 August 2021
Available online 30 August 2021

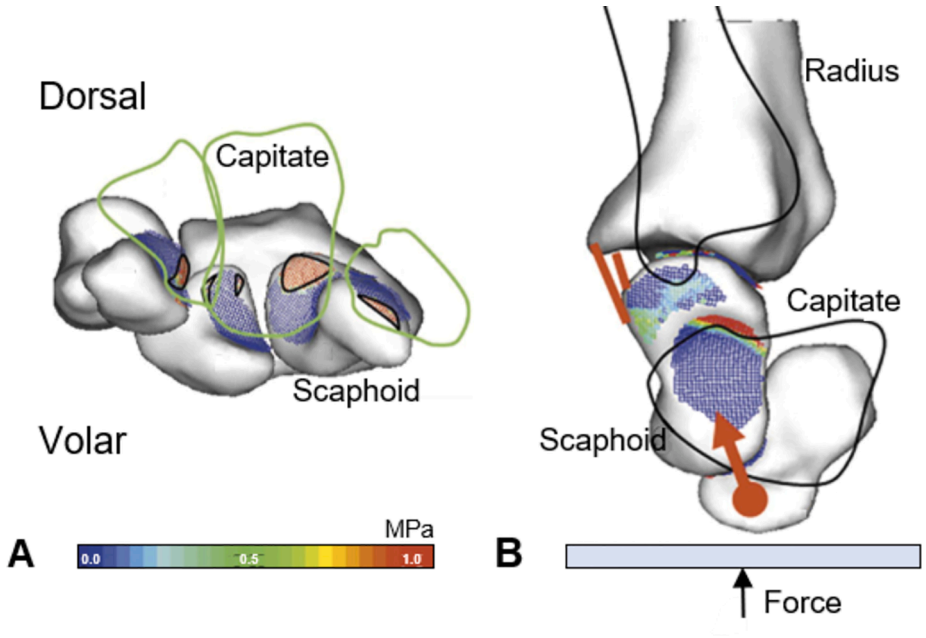

Fig. 1. Wrist mechanics in maximum extension showing A) the concentration of forces on the proximal and distal pole of the scaphoid bone and B) the consequent stabilization of the proximal pole of the scaphoid bone between the distal radius and capitate bone and the force at the distal pole (red arrow) that can cause a bending moment on the scaphoid bone. Adapted from Majima et al., 2008, with permission from Elsevier.

used imaging modalities (Duckworth et al., 2011). Simultaneously, 10–30% of scaphoid fractures remains occult with initial radiography, and the lack of a gold standard modality does not exclude that scaphoid fractures remain occult at follow-up (Brydie and Raby, 2003; Geijer et al., 2011; Hauger et al., 2002; Jenkins et al., 2008; Groves et al., 2006, Memarsadeghi et al., 2006; Tiel-van Buul et al., 1993). There is thus a clear need for an improved diagnosis of scaphoid fractures, and, possibly, identifying factors associated with scaphoid fracture presence may help.

The shape of the scaphoid bone could possibly be such factor. Scaphoid fractures are typically caused by a fall on the outstretched hand with the wrist hyperextended and radially loaded (Duckworth et al., 2012b; Van Tassel et al., 2010; Weber et al., 1978). In maximum extension, external forces become concentrated at the proximal and distal pole of the scaphoid bone (Fig. 1A) (Majima et al., 2008; Weber et al., 1978). The forces at the proximal pole stabilize the proximal part of the scaphoid bone together with wrist ligaments between the distal radius and capitate bone, whereas the forces at the distal pole cause a bending moment due to an offset in the force line of action and the curved shape of the scaphoid bone (Fig. 1B) (Majima et al., 2008; Weber et al., 1978). An excessive bending moment can successively cause a scaphoid fracture, especially at the proximal pole or waist. The shape of the scaphoid bone may play a role in fracture susceptibility after such fall and subsequent loading condition due to its possible influence on bone strength (*e.g.* a thinner and more curved shaped bone may withstand lower bending moments) and on wrist kinematics and loading distributions (*e.g.* by its complex interaction with the surrounding carpal bones and distal radius). Consequently, an association between scaphoid bone shape and the presence of a fracture is possible, also given the variation in anatomy (Van de Giessen et al., 2010), but has not been studied yet.

A reason for this gap may be the complexity to quantify the shape of the scaphoid bone. Attempts to characterize the shape are limited to simplified measures (*e.g.* length, width, presence of specific landmarks) that do not adequately describe the complex three-dimensional shape of the bone (Ceri et al., 2004; Compson et al., 1994). Statistical shape models (SSMs) allow description of a mean shape and shape variation in three dimensions and independent of anatomical landmarks. Previously, scaphoid SSMs have been constructed from radiographs or computed tomography (CT) images and aimed to describe interindividual shape variation, segment individual carpal bones, and investigate skeletal maturity and wrist motion patterns (Adeshina et al., 2017; Anas et al., 2016; Foster et al., 2019; Van de Giessen et al., 2010, 2012). No scaphoid SSMs have been constructed to study the shape of both fractured and non-fractured scaphoid bones. Therefore, the aim of this study was to investigate whether SSM-based shape parameters are associated with fracture presence in patients with a clinically suspected scaphoid fracture. A SSM was constructed from a small set of scans obtained with high-resolution peripheral quantitative CT (HR-pQCT), which we have previously found to allow acquisition of scans of good image quality in patients with a suspected scaphoid fracture and to allow diagnosis of scaphoid fractures with good interobserver agreement and with reveal of fractures that were missed with conventional CT (Bevers et al., 2020; Daniels et al., 2020a,b).

2. Methodology

2.1. Dataset

HR-pQCT imaging was performed of the scaphoid bone in 91 adult male and female patients who consecutively presented at the emergency department of VieCuri Medical Center (Venlo, The Netherlands) with a suspected scaphoid fracture. Study design and population have previously been described in detail (Bevers et al., 2020; Daniels et al., 2020a, b). Briefly, according to the hospital's clinical practice, the patients received conventional plain radiographs at initial presentation, followed by immobilization of the wrist in a polyester cast until follow-up due to suspicion of a scaphoid fracture. At follow-up within 7–10 days after initial presentation, physical re-examination was performed. After written informed consent, the patients underwent HR-pQCT imaging of the scaphoid bone. The HR-pQCT scan (XtremeCT II, Scanco Medical AG, Zürich, Switzerland) constituted a 30.6-mm region (three consecutive stacks) of the wrist covering the entire scaphoid bone. During image acquisition, the wrist was immobilized in the polyester cast with additional removable thumb part for thumb stability and was placed in a standard motion restraining holder. The scans were reconstructed with

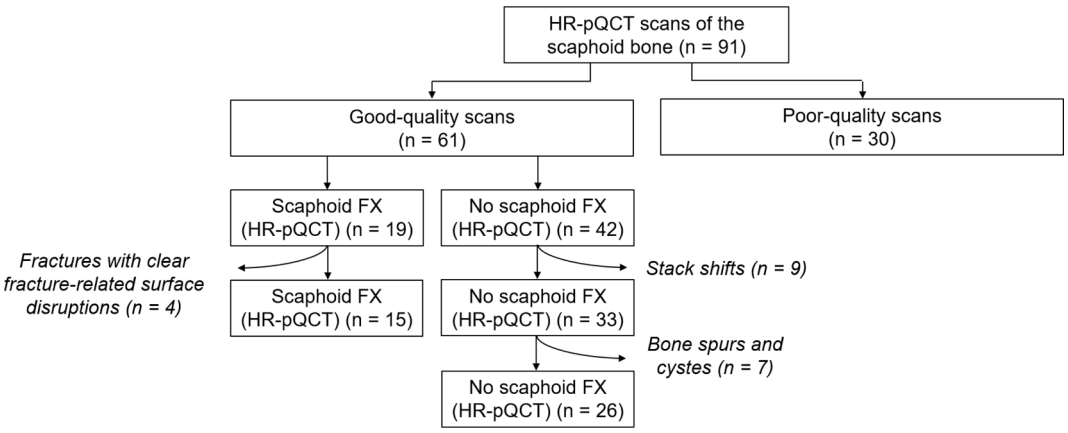

Fig. 2. Flowchart of the high-resolution peripheral quantitative computed tomography (HR-pQCT) scans of scaphoid bones diagnosed as fractured or non-fractured on HR-pQCT used to construct a statistical shape model. FX represents fracture.

an isotropic voxel size of 61 μm. Scan quality was evaluated *post hoc* by applying the clinically used grading system for HR-pQCT scans to multiple full-resolution slices of the scans to grade the quality of each stack of a scan (Bevers et al., 2020).

Only scans with three good-quality stacks were used to construct the SSM (Fig. 2) as motion artefacts in poor-quality scans could affect bone shape. Sixty-one of the 91 scans were of good quality of which 19 scans were of fractured scaphoid bones and 42 of non-fractured scaphoid bones based on diagnosis on HR-pQCT by an experienced radiologist. Four of the 19 scans with a scaphoid fracture were excluded because of fracture-related discontinuities visible in the bone surface (*e.g.* fracture displacements). Nine of the 42 scans without scaphoid fracture were excluded because of stack shifts affecting the shape of the bone surface and seven others because of bone spurs and cysts. In total, 41 scans were used for SSM construction, 15 of which were of fractured scaphoid bones and 26 of non-fractured scaphoid bones.

2.2. SSM construction

2.2.1. Contouring and meshing

The scaphoid bones on the HR-pQCT scans were contoured and subsequently meshed prior to SSM construction. The contouring has been described earlier (Bevers et al., 2020). Briefly, coarse pre-contours were drawn by hand, which were used as starting point for an automatic contouring algorithm that has originally been designed for the radius and tibia and is provided by the manufacturer of the scanner. If necessary, the contours were manually corrected when visually deviating from the outer bone margins to remove any spurs or other erroneous irregularities in the contours. The final contours were converted to three-dimensional masks (Mimics Research 18.0, Materialise NV, Heverlee, Belgium), which in turn were converted to triangular surface meshes with a maximum triangular edge length of 0.5 mm (3-Matic Research 10.0, Materialise NV, Heverlee, Belgium). The meshes were smoothened in MATLAB (Version R2019b, The MathWorks Inc. USA) using Taubin's non-shrinking surface smoothening (Taubin, 1995). To determine the interobserver variability of the contouring process, a subset of eight scans was also contoured by a second investigator following the same procedure. The median of the mean and maximum distance between the contours of this subset were 0.004 mm and 0.245 mm, respectively.

2.2.2. Mesh registration

The smoothened meshes were registered using a publicly available MATLAB-algorithm (Manu, 2019a) that has been described in mathematical detail earlier (Audenaert et al., 2019). Briefly, one mesh was randomly selected as template mesh (*source*) to which the other meshes (*targets*) were rigidly and subsequently non-rigidly registered. Rigid registration consisted of a pre-alignment of *target* and *source* according to their principal axes of inertia, which was successively optimized using an adapted rigid iterative closest point (ICP-) approach that minimized the distance between bidirectional point correspondences of *target* and *source* (Audenaert et al., 2019; Marzola et al., 2020). The ~ 5% largest distances were excluded to overcome unnatural registrations. The original algorithm was expanded with a visual inspection of the pre-alignment and subsequent correction if needed due to the possible lack of clear principal axes in the scaphoid bones. The remaining distances were further minimized by a non-rigid transformation function that was iteratively optimized. The optimized transformation function was refined by an iteratively optimized weighted locally rigid deformation that was applied to the entire mesh to finalize the registration.

2.2.3. SSM construction

The registered meshes were used to construct and optimize the SSM using a publicly available MATLAB-code (Manu, 2019b). Generalized Procrustes alignment was used to align all meshes, followed by principal component analysis (PCA) to describe the statistical mean shape and shape variance among the aligned meshes by forty (*i.e.* the number of meshes minus one) independent shape modes. The SSM was optimized by using the initial SSM as *a priori* information for the construction of a new SSM. For this purpose, the initial SSM plus its first shape mode were fitted to all original meshes (*i.e.* both *targets* and *source*) to predict the shape of these meshes. Only the first mode was used for this prediction as it explains the largest shape variance among the scaphoid bones. The predicted meshes were then used as individual template meshes to which corresponding original meshes were registered and subsequently used to construct a new SSM, both using the above described algorithms. By replacing the initially used *source* mesh with the individual template meshes, possible bias due to using one randomly selected mesh as *source* was removed, and the proportion of variance explained by each shape mode was increased.

2.2.4. Model accuracy

Accuracy of the optimized SSM was quantified. Each registered mesh was aligned with the SSM excluding ~ 5% of the mesh points with the largest distances, and root-mean-squared errors (RMSEs) were calculated of the remaining distances between the mesh points of the aligned mesh and the SSM. The RMSEs of each mesh were averaged to determine a mean RMSE per mesh, which were averaged to determine an overall RMSE. The number of shape modes included in the SSM for alignment was varied from one to all forty, and an overall RMSE was computed for each number of modes included.

Table 1
Demographics of the patients with and without a scaphoid fracture.

Demographic	Scaphoid fracture (n = 15)	No scaphoid fracture (n = 26)	p-value
Men, n (%)	7 (46.7)	13 (50.0)	0.837
Age, median (IQR)	38 (28.0)	47 (38.3)	0.129
High-impact fall, n (%)	11 (73.3)	15 (57.7)	0.317

2.3. Statistical analysis

All statistical analyses were performed in R (R Foundation for Statistical Computing, Version R-3.6.2 for Windows, Vienna, Austria). Mann-Whitney U tests and Chi-Square tests were used to determine the significance of age- and gender-differences between patients with and without a fracture. Logistic regression models were constructed with shape modes as predictor variable and fracture presence as dependent variable to investigate the association between fracture presence and shape modes. The shape modes are orthogonal and statistically independent due to the mathematical nature of PCA, so multiple shape modes could be combined in one regression model. Forward stepwise selection using the Wald-test was used to select the modes to include, selecting from only those modes that cumulatively explained $\geq$ 95% of the shape variance. Bootstrapping was performed with one-thousand repetitions to internally validate the regression model and to prevent overestimation of the model performance. The shrinkage factor resulting from the bootstrapping was used to shrink the regression coefficients of the original regression model to account for potential overfitting. The final regression model consisted of the shrunk coefficients and a re-estimated intercept and satisfied a perfect calibration-in-the-large (*i.e.* agreement between actual fracture proportion in the dataset and mean fracture probabilities predicted by the regression model). Similarly, regression models were constructed with the same selected shape modes and age or gender. Finally, regression models with only age or gender were constructed.

The models were used to classify the 41 scaphoid bones as fractured or non-fractured. Youden's Index J (J = sensitivity + specificity − 1) was determined for various cut-off values for the fracture probability, and the optimal cut-off value was defined as the value with the highest J (Figure Supplementary figure 1). The optimal cut-off value, rounded to the nearest 0.05, was used for the classification, which was compared to the diagnosis on HR-pQCT. Sensitivity, specificity, and accuracy were computed including 95% Clopper-Pearson intervals (Clopper and Pearson, 1934). Positive and negative predictive values (PPV and NPV, respectively) were computed including standard logit 95% confidence intervals (Mercaldo et al., 2007), and also area under the receiver operator characteristic (ROC-) curve (AUC) was calculated. To compute accuracy, PPV, and NPV, the true fracture rate was set to that of the entire dataset (*i.e.* 24 of 91; 26%). Akaike information criterion (AIC) was determined for the regression models to compare the quality of each regression model.

3. Results

The patient characteristics are outlined in Table 1. Age was not significantly different between the patients with and without a scaphoid fracture, and also gender was evenly distributed among the two groups. The proportion of patients with a high-impact fall was not significantly different between those with and those without a scaphoid fracture. According to Herbert's classification system, the included fracture types constituted types A1 (5x), A2 (4x), B1 (2x), B2 (1x), and B3 (3x) based on diagnosis on HR-pQCT by an experienced radiologist (Herbert and Fisher, 1984).

3.1. SSM description

The first shape mode predominantly described the variance in bone size and explained 72.1% of the total shape variance (Fig. 3A). The second and third mode explained an additional 6.3% and 4.2%, respectively of the shape variance with respect to their previous modes, and the first five modes cumulatively explained 87.8% of the shape variance. The shape variance described by these first five modes is visualized in Fig. 4A. The first 13 modes explained 95.3% of the shape variance, and the additional shape variance explained by the next modes was < 0.5% with respect to their previous modes.

The accuracy of the SSM increased with the number of modes included (Fig. 3B). The RMSE was 0.48 ± 0.17 mm when only the first

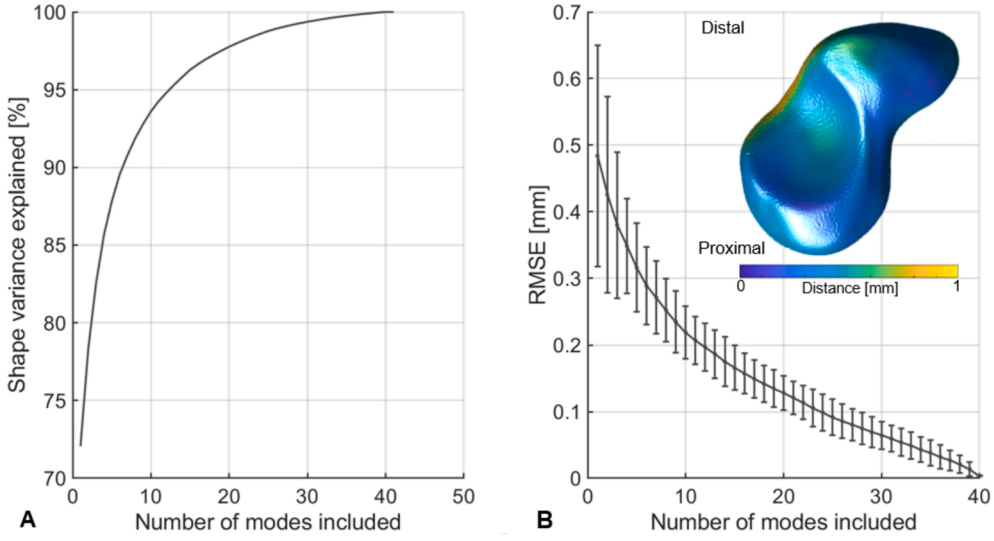

Fig. 3. A) Compactness and B) accuracy of the statistical shape model of the scaphoid bone based on 41 high-resolution peripheral quantitative computed tomography scans of fractured and non-fractured scaphoid bones. The inserted image in B) shows a colormap of the average distance between the included scaphoid bones and their estimated shape from the statistical shape model. RMSE is root-mean-squared error.

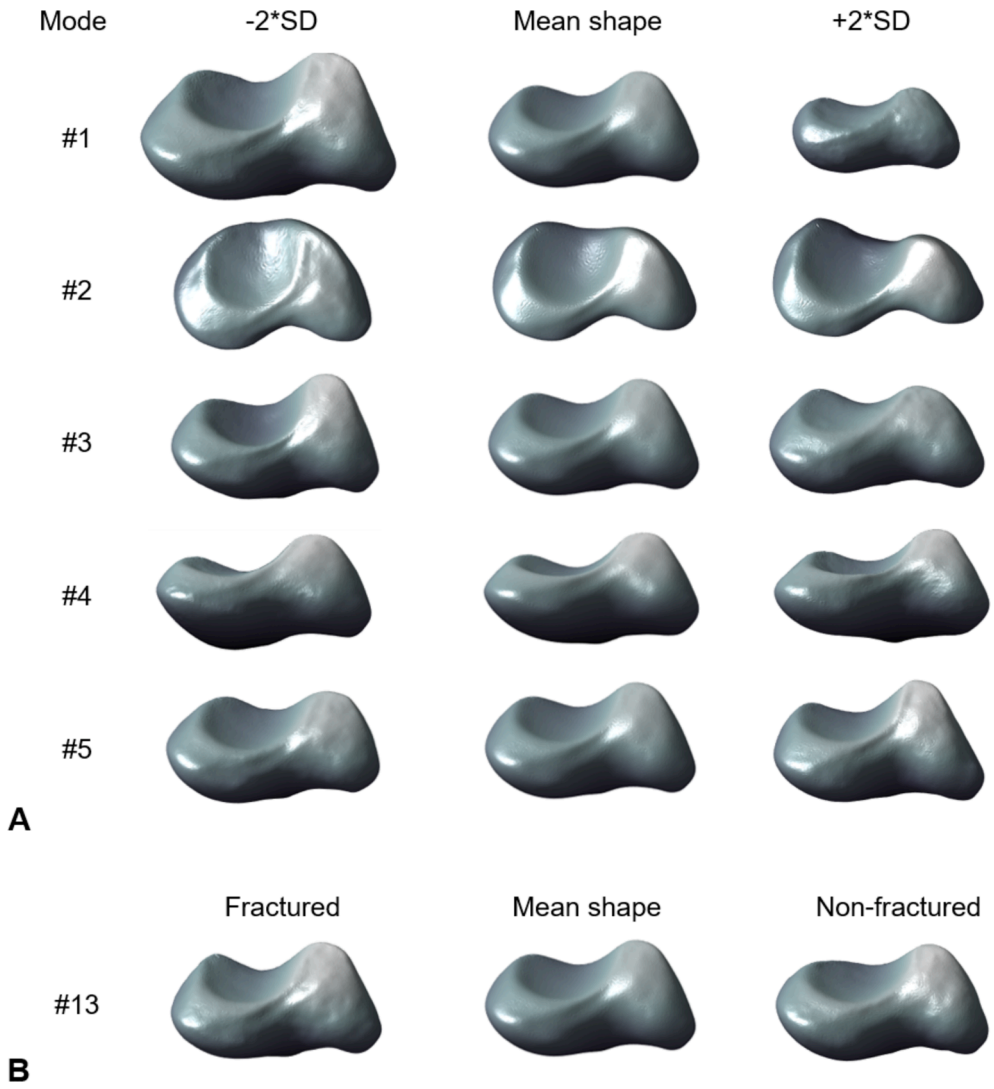

Fig. 4. A) The first five shape modes of the statistical shape model that cumulatively explained 87.8% of the shape variation among the 41 scaphoid bones used to construct the model. Mean shape and ± 2 times the standard deviation (SD) of the modes are visualized. B) Shape variance explained by the thirteenth shape mode of the statistical shape model that was significantly different between the fractured and non-fractured scaphoid bones.

mode was included and decreased to 0.19 ± 0.036 mm when the first 13 modes were included. It approached zero when all forty modes were included (0.0035 ± 0.00027 mm). The distance between the original included scaphoid bones and their estimated shape from the SSM was largest at the dorsal boundary of the facet articulating with the capitate bone (Fig. 3B).

3.2. Classification performance

The first 13 shape modes were pre-selected for the construction of logistic regression models because they together explained ≥ 95% (95.3%) of the shape variance, and the forward selection procedure selected four of these modes (modes #13, #8, #7, #3). The first of these modes (mode #13) was significantly different between the fractured and non-fractured scaphoid bones (Fig. 4B), but it explained < 1% of the shape variance among the included bones. A regression model with the four selected shape modes had a significant OR of 8.25 and an AUC of 72.3%, which were both considerably higher compared to regression models with age or gender as predictor variable (Table 2, Fig. 5). Also the proportion of correctly classified bones (75.6%) was considerably higher for this model compared to the regression models with age or gender. With an optimal cut-off of 0.45, specificity and NPV were > 80% (Table 3). Accounting for age or gender considerably increased OR of the regression model with the four modes. Accounting for age also increased AUC due to a higher sensitivity and specificity for sensitivities > 75%. The proportion of correctly classified bones increased slightly (Table 2, Fig. 5). Accounting for gender did not change AUC but slightly increased the proportion of correctly classified bones due to an increased proportion of correctly classified non-fractured scaphoid bones (Table 2, Fig. 5).

4. Discussion

The aim of this study was to investigate whether shape parameters from a SSM of the scaphoid bone are associated with the presence of a scaphoid fracture in patients with a clinically suspected fracture. The first five out of forty shape modes cumulatively explained 87.8% of the shape variance among the scaphoid bones, and the first 13 modes explained > 95% of the variance. A logistic regression model with four out of the first 13 modes as predictor variable resulted in a significant OR of 8.25 and an AUC of 72.3%. It correctly classified 75.6% of the scaphoid bones (fractured: 60.0%, non-fractured: 84.6%) when using a cut-off value of 0.45 for fracture probability.

These results suggest that there may be an association between

Table 2
Characteristics of five logistic regression models with scaphoid fracture presence as dependent variable.

Regression model predictor(s)	AIC [-]	AUC [%]	Optimal cut-off [-]	OR (95%-CI) [-]	Correct classification [- (%)]	
					Fracture (n = 15)	No fracture (n = 26)
Age (1 yr.)	53.3	66.4	0.25	5.57 (1.04–29.8)*	13 (86.7)	12 (46.2)
Gender (men)	55.8	50.0	0.35	1.71 (0.03–90.6)	0 (0.0)	26 (100.0)
Shape mode (four; Wald)	42.9	72.3	0.45	8.25 (1.87–36.4)*	9 (60.0)	22 (84.6)
Shape mode (four; Wald) + Age	39.1	81.3	0.30	31.5 (3.51–282)*	14 (93.3)	18 (69.2)
Shape mode (four; Wald) + Gender	43.6	71.4	0.55	21.9 (2.33–206)*	7 (46.7)	25 (96.2)

AIC is Akaike information criterion; AUC is area under the receiver operating characteristic (ROC) curve; and OR is odds ratio.
* denotes $p < 0.05$.

scaphoid bone shape and fracture presence in patients with a suspected fracture. This could be explained by several factors. One factor may be the possible influence of the shape of the bone on its strength. During a fall on the outstretched hand, the scaphoid bone experiences a combination of compression and bending, which causes a bending moment on the scaphoid bone (Majima et al., 2008; Weber et al., 1978). An excessive bending moment can cause a fracture, and a thinner and more curved bone shape could possibly lower the ability to withstand such moment, subsequently increasing fracture susceptibility after a fall. Additionally, the shape of the scaphoid bone may contribute to the amount of force that the bone has to withstand during a fall due to the complex interaction of the scaphoid bone with the surrounding bones and its bridging function of the proximal and distal carpal row, which both could influence wrist kinematics and subsequently loading distributions. Due to the mathematical nature of shape modes and the explorative nature of this study, it was difficult and beyond the scope of the study to anatomically explain shape differences between fractured and non-fractured scaphoid bones in relation to fracture mechanics, but it is encouraged to investigate this in future studies.

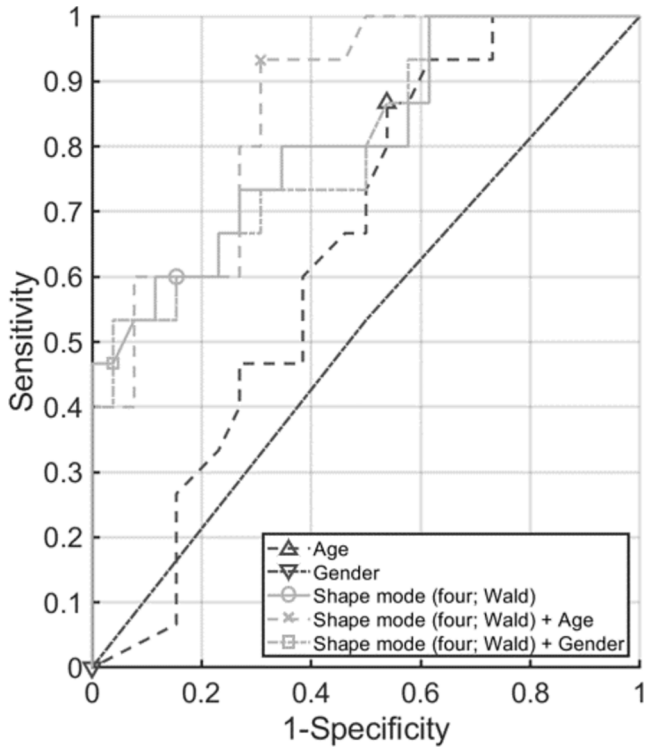

Fig. 5. Receiver operating characteristic curves of logistic regression models with scaphoid fracture presence as dependent variable and age, gender, the four shape modes selected with Forward stepwise selection using the Wald-test or the four shape modes + age/gender as predictor variable(s). The symbols in the curves represent the optimal cut-off value for the fracture probabilities estimated by the logistic regression models, rounded to the nearest 0.05 and used to quantify the classification performance of the models.

Our SSM was based on HR-pQCT scans, which have a higher resolution than scans made with imaging modalities currently used for scaphoid fracture diagnosis, such as radiography, CT, or magnetic resonance imaging (MRI). The first five shape modes of our SSM explained a larger proportion of shape variance among the included fractured and non-fractured scaphoid bones than a SSM from CT-scans of non-fractured scaphoid bones (Van de Giessen et al., 2010), indicating that our SSM requires less shape modes to explain a certain shape variance than the CT-based SSM in literature. It is however unlikely that the higher resolution of the HR-pQCT scans contributed to this difference as the meshes used for our SSM had an maximum edge length of 0.5 mm, which is a resolution that can also be obtained by clinical whole-body CT-scanners. Furthermore, for the CT-based SSM, the scaphoid bones were scaled as part of the registration, thereby removing variation in bone size and consequently not having a shape mode explaining this variation, whereas we did not scale the bones, leading to our first shape mode that explained > 70% of shape variance mainly arisen from bone size differences. It was beyond the scope of the current study to investigate whether shape differences between fractured and non-fractured scaphoid bones may also be captured with CT, radiography, or MRI, and whether SSMs based on lower-resolution scans allow discrimination between fractured and non-fractured scaphoid bones.

Although not clinically usable given the current prediction rate (75.6%), SSM-based shape could possibly be when incorporated in clinical decision rules together with other patient data when further studied in larger datasets. The use of clinical prediction rules has been suggested as a strategy to improve the challenging diagnosis of scaphoid fractures (Duckworth et al., 2011). Various prediction rules have been investigated earlier for scaphoid fracture diagnosis and combined pre-imaging characteristics, such as physical examination findings, demographic factors, and wrist range of motion and grip strength parameters (Duckworth et al., 2012a; Mallee et al., 2020; Parvizi et al., 1998; Rhemrev et al., 2010). Imaging-based bone shape could possibly

Table 3
Classification performance of the logistic regression model with four shape modes as predictor variable selected with Forward stepwise selection using the Wald-test and a cut-off value of 0.45. Diagnosis based on HR-pQCT scans was used as true reference.

	True scaphoid fracture	No scaphoid fracture	Total
Shape modes +	9	4	13
Shape modes -	6	22	28
Total	15	26	41
Sensitivity	60.0 (32.3–83.7)		
Specificity	84.6 (65.1–95.6)		
PPV	57.8 (33.7–78.7)		
NPV	85.8 (76.0–92.0)		
Accuracy	78.2 (62.6–89.6)		
AUC	72.3		

PPV and NPV are positive and negative predictive value, respectively.
For computation of accuracy, PPV, and NPV, a true fracture rate of 26% was used.
Values are expressed as percentages with 95% confidence intervals.

further contribute to discriminating between patients with and without a scaphoid fracture, strengthened by having included only fractures without clearly visible fracture-related surface irregularities, which are more likely to be missed than fractures with more clear surface discontinuities. Furthermore, the lack of significant differences in age and in the proportion of men and high-impact falls between those with and without a scaphoid fracture suggests the possible discriminative ability of bone shape to be independent of age, gender, and trauma magnitude. Body weight was not measured but could possibly influence trauma magnitude. Nevertheless, the current algorithm needs to be validated in larger series to investigate the robustness of the association between bone shape and fracture presence on HR-pQCT or conventional imaging modalities. Also, the possibility to use the bone shape in clinical prediction rules requires further study.

Bone mineral density (BMD) is another image-based characteristic that can be integrated in a statistical model. Statistical shape and density models have for example been developed of the proximal femur to investigate whether shape and density modes of these models can discriminate between patients without a hip fracture or with an incident or contralateral hip fracture (Bredbenner et al., 2014; Goodyear et al., 2013; Whitmarsh et al., 2011). The rationale of including BMD in such studies is related to findings that BMD, usually assessed with dual-energy X-ray absorptiometry (DXA), is associated with osteoporotic fracture risk. Scaphoid fractures represent however a different patient population with generally younger and more active individuals and a different fracture mechanism. The role of BMD on fracture risk or fracture presence is therefore less likely in the scaphoid fracture population compared to the population sustaining an osteoporotic fracture. Bone shape plays in contrast a more likely role in scaphoid fractures due to the complex shape of the scaphoid bone and its anatomical location in the wrist. We therefore did not include BMD but only bone shape in our statistical model.

This study has several limitations. First, the small dataset did not allow differentiation between scaphoid fracture types in constructing the SSM or the logistic regression models, while some of the included fracture types can be more devastating to miss than others (*e.g.* proximal pole fractures, Herbert's type B3) and may be considered clinically more relevant. Moreover, the small dataset increased the risk for overestimating classification performance due to overfitting. A general rule of thumb is to limit the number of predictor variables in a logistic regression model to one per ten events (*i.e.* fractures), which implies overfitting in the regression model with four shape modes. A regression model with one of the four selected modes individually does satisfy this rule of thumb and allowed moderate to fair classification for modes #13 and #8 (Supplementary Table 1). Mode #13 explained however $< 1\%$ of the total shape variance among the included scaphoid bones, which may suggest the possibility of being a finding related to the small sample size. Mode #8 explained 1.1% of total shape variance. Particular (and small) shape variations could theoretically and anatomically allow discrimination between fractured and non-fractured scaphoid bones, while larger shape variations do not have to (*e.g.* bone size, mode #1, given the even distribution of gender), but study in larger datasets is needed to further investigate the association between bone shape and scaphoid fracture presence. Second, we used both left and right scaphoid bones of both men and women for the construction of our SSM. Using left and right bones may be justified as the shape of the scaphoid bone appears bilaterally symmetric (Ten Berg et al., 2015). In contrast, gender-related shape variances (*e.g.* size) have been found in the scaphoid bone (Ceri et al., 2004; Heinzelmann et al., 2007; Letta et al., 2014; Patterson et al., 1995). However, in our study, gender was evenly distributed among the fractured and non-fractured scaphoid bones and accounted for in the logistic regression models, which justifies the inclusion of both male and female scaphoid bones. Third, due to the novelty of applying HR-pQCT imaging to the scaphoid bone, data on the intra- and interobserver variability of manually correcting the contours are lacking and warrant further study. Finally, as mentioned earlier, we used HR-pQCT scans for SSM construction, which have a higher resolution than imaging modalities currently used for scaphoid fracture diagnosis. Although the used mesh edge lengths are obtainable with whole-body CT, it has to be investigated whether bone shape from lower-resolution scans is associated with fracture presence.

To conclude, this exploratory study showed that the shape of the scaphoid bone quantified with a SSM from HR-pQCT scans seems to be associated with the presence of a scaphoid fracture in patients with a clinically suspected fracture. Further studies are needed to investigate this association, its relationship with fracture mechanics, and possible clinical implications of such association for scaphoid fracture diagnosis.

Declaration of Competing Interest

The authors declare that they have no known competing financial interests or personal relationships that could have appeared to influence the work reported in this paper.

Acknowledgements

This study was supported by the research foundation of VieCuri Medical Center Noord-Limburg, The Netherlands.

Appendix A. Supplementary material

Supplementary data to this article can be found online at https://doi.org/10.1016/j.jbiomech.2021.110726.

References

Adeshina, S.A., Cootes, T.F., Adams, J., 2017. Automatic determination of skeletal maturity using statistical models of appearance. Int. J. Comput. Tech. 4, 1–11.
Anas, E.M.A., Rasoulian, A., Seitel, A., Darras, K., Wilson, D., St John, P., Pichora, D., Mousavi, P., Rohling, R., Abolmaesumi, P., 2016. Automatic Segmentation of Wrist Bones in CT Using a Statistical Wrist Shape + Pose Model. IEEE Trans. Med. Imaging 35, 1789–1801.
Audenaert, E.A., Van Houcke, J., Almeida, D.F., Paelinck, L., Peiffer, M., Steenackers, G., Vandermeulen, D., 2019. Cascaded statistical shape model based segmentation of the full lower limb in CT. Comput. Methods Biomech. Biomed. Eng. 22 (6), 644–657.
Bevers, M.S.A.M., Daniels, A.M., Wyers, C.E., van Rietbergen, B., Geusens, P.P.M.M., Kaarsemaker, S., Janzing, H.M.J., Hannemann, P.F.W., Poeze, M., van den Bergh, J. P.W., 2020. The Feasibility of High-Resolution Peripheral Quantitative Computed Tomography (HR-pQCT) in Patients with Suspected Scaphoid Fractures. J. Clin. Densitometry 23 (3), 432–442.
Bredbenner, T.L., Mason, R.L., Havill, L.M., Orwoll, E.S., Nicolella, D.P., 2014. Fracture risk predictions based on statistical shape and density modeling of the proximal femur. J. Bone Miner. Res. 29 (9), 2090–2100.
Brydie, A., Raby, N., 2003. Early MRI in the management of clinical scaphoid fracture. British J. Radiol. 76 (905), 296–300.
Ceri, N., Korman, E., Gunal, I., Tetik, S., 2004. The morphological and morphometric features of the scaphoid. J. Hand Surg.: British Eur. 29 (4), 393–398.
CLOPPER, C.J., PEARSON, E.S., 1934. The Use of Confidence or Fiducial Limits Illustrated in the Case of the Binomial. Biometrika 26 (4), 404–413.
Compson, J.P., Waterman, J.K., Heatley, F.W., 1994. The radiological anatomy of the scaphoid. Part 1: Osteology. J. Hand Surg.: British Eur. 19 (2), 183–187.
Daniels, A.M., Bevers, M.S.A.M., Sassen, S., Wyers, C.E., Van Rietbergen, B., Geusens, P. P.M.M., Kaarsemaker, S., Hannemann, P.F.W., Poeze, M., Van den Bergh, J.P., Janzing, H.M.J., 2020a. Improved detection of scaphoid fractures with High Resolution peripheral Quantitative Computed Tomography compared to conventional CT. J. Bone Joint Surg. Am. 102, 2138–2145.
Daniels, A.M., Wyers, C.E., Janzing, H.M.J., Sassen, S., Loeffen, D., Kaarsemaker, S., van Rietbergen, B., Hannemann, P.F.W., Poeze, M., van den Bergh, J.P., 2020b. The interobserver reliability of the diagnosis and classification of scaphoid fractures using high-resolution peripheral quantitative CT. Bone Joint J. 102-B (4), 478–484.
Duckworth, A.D., Buijze, G.A., Moran, M., Gray, A., Court-Brown, C.M., Ring, D., McQueen, M.M., 2012a. Predictors of fracture following suspected injury to the scaphoid. J. Bone Joint Surg. British 94-B (7), 961–968.
Duckworth, A.D., Jenkins, P.J., Aitken, S.A., Clement, N.D., Court-Brown, C.M., McQueen, M.M., 2012b. Scaphoid fracture epidemiology. J. Trauma Acute Care Surg. 72, E41–E45.
Duckworth, A.D., Ring, D., McQueen, M.M., 2011. Assessment of the suspected fracture of the scaphoid. J. Bone Joint Surg. British 93-B (6), 713–719.
Foster, B.H., Shaw, C.B., Boutin, R.D., Joshi, A.A., Bayne, C.O., Szabo, R.M., Chaudhari, A.J., 2019. A principal component analysis-based framework for statistical modeling of bone displacement during wrist maneuvers. J. Biomech. 85, 173–181.

Geijer, M., Börjesson, A.M., Göthlin, J.H., 2011. Clinical utility of tomosynthesis in suspected scaphoid fracture. Pilot Study. Skeletal Radiol. 40 (7), 863–867.
Goodyear, S.R., Barr, R.J., McCloskey, E., Alesci, S., Aspden, R.M., Reid, D.M., Gregory, J.S., 2013. Can we improve the prediction of hip fracture by assessing bone structure using shape and appearance modelling? Bone 53 (1), 188–193.
Groves, A.M., Kayani, I., Syed, R., Hutton, B.F., Bearcroft, P.P.W., Dixon, A.K., Ell, P.J., 2006. An international survey of hospital practice in the imaging of acute scaphoid trauma. Am. J. Roentgenol. 187 (6), 1453–1456.
Hauger, O., Bonnefoy, O., Moinard, M., Bersani, D., Diard, F., 2002. Occult fractures of the waist of the scaphoid: early diagnosis by high-spatial-resolution sonography. Am. J. Roentgenol. 178 (5), 1239–1245.
Heinzelmann, A.D., Archer, G., Bindra, R.R., 2007. Anthropometry of the human scaphoid. J. Hand Surg. 32 (7), 1005–1008.
Herbert, T.J., Fisher, W.E., 1984. Management of the fractured scaphoid using a new bone screw. J. Bone Joint Surg. British 66-B (1), 114–123.
Hove, L.M., 1999. Epidemiology of Scaphoid Fractures in Bergen, Norway. Scand. J. Plast. Reconstr. Surg. Hand Surg. 33 (4), 423–426.
Jenkins, P.J., Slade, K., Huntley, J.S., Robinson, C.M., 2008. A comparative analysis of the accuracy, diagnostic uncertainty and cost of imaging modalities in suspected scaphoid fractures. Injury 39 (7), 768–774.
Letta, C., Schweizer, A., Fürnstahl, P., 2014. Quantification of contralateral differences of the scaphoid: a comparison of bone geometry in three dimensions. Anat. Res. Int. 2014, 1–5.
Majima, M., Horii, E., Matsuki, H., Hirata, H., Genda, E., 2008. Load transmission through the wrist in the extended position. J. Hand Surg.: Am. 33 (2), 182–188.
Mallee, W.H., Walenkamp, M.M.J., Mulders, M.A.M., Goslings, J.C., Schep, N.W.L., 2020. Detecting scaphoid fractures in wrist injury: a clinical decision rule. Arch. Orthop. Trauma Surg. 140 (4), 575–581.
Manu, 2019a. nonrigidICP (https://www.mathworks.com/matlabcentral/fileexchange/41396), MATLAB Central File Exchange. Retrieved April 29, 2019.
Manu, 2019b. Shape Model Builder (https://www.mathworks.com/matlabcentral/fileexchange/49940), MATLAB Central File Exchange. Retrieved April 29, 2019.
Marzola, A., Robilotta, C., Volpe, Y., Governi, L., Furferi, R., 2020. Statistical Shape Model: comparison between ICP and CPD algorithms on medical applications. Int. J. Interact. Des. Manuf. (IJIDeM) 15 (1), 85–89.
Memarsadeghi, M., Breitenseher, M.J., Schaefer-Prokop, C., Weber, M., Aldrian, S., Gäbler, C., Prokop, M., 2006. Occult scaphoid fractures: comparison of multidetector CT and MR imaging—initial experience. Radiology 240 (1), 169–176.
Mercaldo, N.D., Lau, K.F., Zhou, X.H., 2007. Confidence intervals for predictive values with an emphasis to case-control studies. Stat. Med. 26 (10), 2170–2183.
PARVIZI, J., WAYMAN, J., KELLY, P., MORAN, C.G., 1998. Combining the clinical signs improves diagnosis of scaphoid fractures: a prospective study with follow-up. J. Hand Surg.: British Eur. 23 (3), 324–327.
Patterson, R.M., Elder, K.W., Viegas, S.F., Buford, W.L., 1995. Carpal bone anatomy measured by computer analysis of three-dimensional reconstructions of computed tomography images. J. Hand Surg.: Am. 20 (6), 923–929.
Rhemrev, S.J., Beeres, F.J.P., van Leerdam, R.H., Hogervorst, M., Ring, D., 2010. Clinical prediction rule for suspected scaphoid fractures: A Prospective Cohort Study. Injury 41 (10), 1026–1030.
Taubin, G., 1995. A signal processing approach to fair surface design. In Proceedings of the 22nd annual conference on Computer graphics and interactive techniques. Los Angeles, United States.
ten Berg, P.W.L., Dobbe, J.G.G., Strackee, S.D., Streekstra, G.J., 2015. Three-dimensional assessment of bilateral symmetry of the scaphoid: an anatomic study. Biomed Res. Int. 2015, 1–6.
Tiel-van Buul, M.M., van Beek, E.J., Broekhuizen, A.H., Bakker, A.J., Bos, K.E., van Royen, E.A., 1993. Radiography and scintigraphy of suspected scaphoid fracture. A long-term study in 160 patients. J. Bone Joint Surg. British 75-B (1), 61–65.
van de Giessen, M., Foumani, M., Streekstra, G.J., Strackee, S.D., Maas, M., van Vliet, L. J., Grimbergen, K.A., Vos, F.M., 2010. Statistical descriptions of scaphoid and lunate bone shapes. J. Biomech. 43 (8), 1463–1469.
van de Giessen, M., Foumani, M., Vos, F.M., Strackee, S.D., Maas, M., Van Vliet, L.J., Grimbergen, C.A., Streekstra, G.J., 2012. A 4D statistical model of wrist bone motion patterns. IEEE Trans. Med. Imaging 31 (3), 613–625.
VAN ONSELEN, E.B.H., KARIM, R.B., HAGE, J.JORIS., RITT, M.J.P.F., 2003. Prevalence and distribution of hand fractures. J. Hand Surg.: British Eur. 28 (5), 491–495.
Van Tassel, D.C., Owens, B.D., Wolf, J.M., 2010. Incidence estimates and demographics of scaphoid fracture in the U.S. population. J. Hand Surg.: Am. 35 (8), 1242–1245.
Weber, E.R., Chao, E.Y., 1978. An experimental approach to the mechanism of scaphoid waist fractures. J. Hand Surg.: Am. 3 (2), 142–148.
Whitmarsh, T., Fritscher, K. D., Humbert, L., Del Rio Barquero, L. M., Roth, T., Kammerlander, C., Blauth, M., Schubert, R., Frangi, A. F., 2011. A statistical model of shape and bone mineral density distribution of the proximal femur for fracture risk assessment. In Proceedings of the 14th International Conference on Medical Image Computing and Computer-Assisted Intervention – MICCAI 2011. Toronto, Canada.